MRI Contrast Agent

DOI: 10.1002/anie.201100562

Simple Synthesis and Functionalization of Iron Nanoparticles for Magnetic Resonance Imaging**

*Soshan Cheong, Peter Ferguson, Kirk W. Feindel, Ian F. Hermans, Paul T. Callaghan, Claire Meyer, Angela Slocombe, Chia-Hao Su, Fong-Yu Cheng, Chen-Sheng Yeh, Bridget Ingham, Michael F. Toney, and Richard D. Tilley**

Magnetic nanoparticles (NPs) are increasingly important in many biomedical applications, such as drug delivery, hyperthermia, and magnetic resonance imaging (MRI) contrast enhancement.[1] For MRI, iron oxide NPs are the only commercial T_2 or negative contrast agents, due to their biocompatibility and ease of synthesis[2] and research in the area is highly active.[3] The efficacy of these contrast agents depends mainly on the surface chemistry and magnetic properties of the NPs.[1] Materials with larger magnetization could induce more efficient transverse (T_2) relaxation of protons and result in greater contrast enhancement.[4] As iron has the highest saturation magnetization at room temperature among all elements,[5] and is biocompatible, it is an ideal candidate for MRI contrast enhancement. Nevertheless, the development of using iron NPs for magnetic applications has been challenging and limited compared to those of its oxides, due to the difficulty in preparing stable iron NPs with simple synthesis methods and precursors.[5,6]

Under ambient conditions, iron NPs of 8 nm or smaller oxidize completely upon exposure to air.[7] For larger NPs, an oxide shell of 3–4 nm forms instantly on the surface, forming iron/iron oxide core/shell NPs. Groundbreaking studies for the synthesis of iron NPs of larger than 8 nm has largely been achieved by decomposition of iron pentacarbonyl, $[Fe(CO)_5]$.[6,8] Additional reports include the use of other precursors in forming iron nanocubes.[9] However, all of these processes are limited in terms of ease of synthesis and scalability; $[Fe(CO)_5]$ is volatile and highly toxic,[5] and other processes involve precursors that are expensive and air-sensitive,[9a] or require high decomposition temperatures.[9b]

Here, we chose an easy to handle iron organometallic sandwich compound as the precursor and prepared single-crystal iron NPs using a simple, low-temperature synthesis method. The iron nanocrystals oxidized naturally to form highly crystalline iron/iron oxide core/shell NPs. The ease of this synthesis facilitates the larger-scale application of stabilized iron NPs. To enable the use of these NPs in biological applications, the NP surface was modified to make the NPs water soluble. The strongly magnetic core/shell NPs are shown to be more effective T_2 contrast agents for in vivo MRI and small tumor detection, compared to pure iron oxides. The successful detection of small tumors in vivo demonstrated here holds a great promise for accurate detection of early metastases in human lymph nodes, which has a large impact on the treatment and prognosis of a range of cancers.

The iron/iron oxide core/shell NPs were prepared by first synthesizing iron nanocrystals by decomposition of the iron precursor $[Fe(C_5H_5)(C_6H_7)]$, in the presence of oleylamine (OLA) stabilizing molecules. The non-carbonyl, sandwich compound was chosen for its simple preparation and ease of decomposition compared to other more stable sandwich compounds such as ferrocene.[10] The synthesis was carried out in a closed reaction vessel[11] under a mild hydrogen atmosphere, at 130 °C. The temperature required was lower than the usual temperature range (150–300 °C) needed for decomposition of other iron precursors in previous studies. Once

[*] Dr. K. W. Feindel, Prof. P. T. Callaghan, Prof. R. D. Tilley
School of Chemical and Physical Sciences and The MacDiarmid Institute for Advanced Materials and Nanotechnology, Victoria University of Wellington, Wellington 6012 (New Zealand)
Fax: (+64) 4-463-5237
E-mail: richard.tilley@vuw.ac.nz
Dr. S. Cheong,[+] Dr. B. Ingham
Industrial Research Limited and The MacDiarmid Institute for Advanced Materials and Nanotechnology
P. O. Box 31-310, Lower Hutt 5040 (New Zealand)
Dr. P. Ferguson,[+] Dr. I. F. Hermans
Malaghan Institute of Medical Research
P. O. Box 7060, Wellington 6012 (New Zealand)
Dr. C. Meyer
Institut Néel (CNRS and UJF), Grenoble (France)
A. Slocombe
Department of Radiology, Wellington Hospital
Wellington 6021 (New Zealand)
Dr. C.-H. Su
Center for Translational Research in Biomedical Science, Chang Gung Memorial Hospital-Kaohsiung Medical Center
Kaohsiung 833 (Taiwan)
Prof. F.-Y. Cheng, Prof. C.-S. Yeh
Department of Chemistry and Center for Micro/Nano Technology Research, National Cheng Kung University, Tainan 701 (Taiwan)
Dr. M. F. Toney
Stanford Synchrotron Radiation Lightsource, SLAC National Accelerator Laboratory, Menlo Park, CA 94025 (USA)
[+] These authors contributed equally to this work.

[**] This research was supported by the Foundation for Science, Research and Technology through grant PROJ-13733-NMTS. P.F. thanks the Health Research Council and the Wellington Medical Research Foundation for funding. K.W.F. thanks the Natural Sciences and Engineering Research Council of Canada (NSERC) for funding. Portions of this research were carried out at the Stanford Synchrotron Radiation Lightsource, a national user facility operated by Stanford University on behalf of the U.S. Department of Energy, Office of Basic Energy Sciences.

Supporting information for this article is available on the WWW under http://dx.doi.org/10.1002/anie.201100562.

synthesized, the iron nanocrystals were exposed to air to allow oxidation of the surface, forming iron/iron oxide core/shell NPs.

From an application point of view, the oxide layer can be exploited for two purposes: 1) to act as a passivation shell that prevents further oxidation;[7] and 2) to be readily functionalized for various biomedical applications using protocols established for iron oxides.[2b] The stabilizing agent OLA was exchanged with dimercaptosuccinic acid (DMSA) as a capping agent to achieve a stable dispersion in water. DMSA was chosen for its excellent safety profile.[12] Besides, its strong binding of the oxygen-containing acid groups to the iron atoms on the NP surface[13] means the OLA is easily replaced. Upon ligand exchange, the DMSA-coated NPs were readily dispersible in water, and the core/shell structures were stable for at least six months (Supporting Information, Figure S1).

Figure 1a shows a transmission electron microscopy (TEM) image of the spherical, core/shell NPs obtained. The NPs were relatively monodisperse, with an average size of (16 ± 1.5) nm (calculated from 450 NPs). The contrast of the NPs in the image shows a darker core and a lighter shell that reveals a core/shell structure. In high-resolution TEM (HRTEM) images, uniform lattice fringes were observed across the entire NP core, with spacings corresponding to α-Fe(110). For the shell, multiple crystalline domains with lattice spacings matching those of iron oxide were observed (Figure 1b). The X-ray diffraction (XRD) pattern of the sample (Figure 1c) shows diffraction peaks of bulk body-centered cubic iron or α-Fe, and iron oxide of spinel structure, that is, magnetite (Fe_3O_4) or maghemite (γ-Fe_2O_3). The latter is consistent with the native iron oxide film structure previously reported.[14] Using the Scherrer equation,[15] the average crystallite size of α-Fe was estimated from the peak width of Fe(110) and Fe(211), to be (8.9 ± 0.7) nm. This value is close to the average iron core size of (9.0 ± 1.0) nm measured on TEM images. The much broader peaks of iron oxide shows a much smaller average crystallite size, and agree with TEM observation of a 3.2 nm, polycrystalline shell layer of the NPs.

The magnetic hysteresis loop of the sample measured at 300 K (Figure 1d) shows that the iron/iron oxide core/shell NPs exhibit a soft ferromagnetic behavior, with a remnant magnetization of ca. 19 emu g^{-1}(Fe), and a coercivity of ca. 370 Oe. The magnetization values were 140 and 150 emu g^{-1}(Fe) at low (2 T) and high (6 T) fields, respectively (1 T = 10 kOe). This magnetization value is in agreement with other reports of NPs comprising iron core and iron oxide shell of similar size range.[16] The presence of a single-crystal iron core in the sample induces a far higher magnetization compared to iron oxide NPs that typically range from 40–70 emu g^{-1}(Fe).[2]

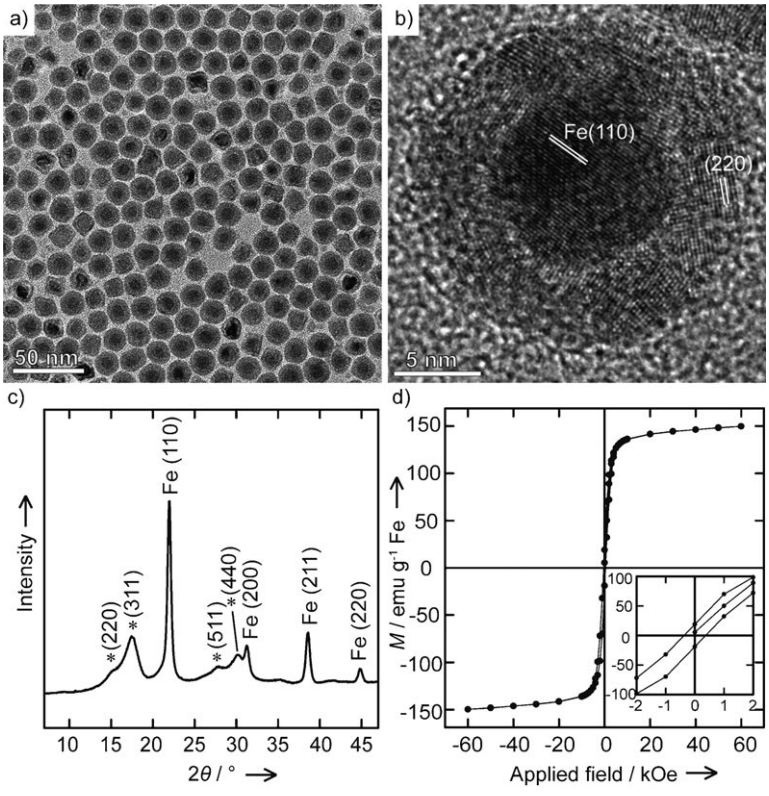

Figure 1. a) TEM image of 16 nm iron/iron oxide core/shell nanoparticles. b) HRTEM image showing a core of single-crystal α-Fe, with {110} planes observed across the core area, and a shell consisting of multiple domains of iron oxide, with {220} planes observed on sections of the shell. c) XRD pattern of the nanoparticles obtained using synchrotron radiation ($\lambda = 0.775$ Å), with diffraction peaks indexed to α-Fe and iron oxide of the spinel phase (*). d) Magnetization (*M*) of the core/shell nanoparticles at 300 K, with inset showing the low-field region.

To compare the properties of the core/shell NPs, DMSA-coated iron oxide NPs of similar size, of average diameter (15 ± 2) nm, were prepared using standard methods.[17] The effectiveness of the NPs as contrast agents was first assessed by measuring T_2-weighted MR images of the NPs at 9.4 T. The NPs were dispersed in agar at different concentrations of iron (in μg(iron) mL^{-1}). As shown in Figure 2a, the core/shell NPs produced much improved negative contrast compared to the oxide NPs at a range of iron concentrations, from 0.5 to 10 μg(Fe) mL^{-1}. In addition, contrast enhancement produced by the core/shell NPs can be detected down to a concentration of 0.5 μg(Fe) mL^{-1}, at which the oxide NPs showed no noticeable difference in the contrast compared the control.

The transverse relaxivity (r_2) of the core/shell NPs was determined for the samples and compared with that of the oxide NPs. (See Figure S2 for a representative plot of T_2 vs. [Fe].) The core/shell NPs had an r_2 of 324 $mM^{-1}s^{-1}$, more than twice that of the oxide NPs, of 145 $mM^{-1}s^{-1}$, as shown in Figure 2b. Contrast improvement relative to that of iron oxide NPs has been reported for amorphous, iron-based core/shell NPs of similar sizes.[18] However, little improvement was observed for the r_2 value indicating the importance of the single-crystal α-Fe core in our samples. This increase in r_2 indicates a significantly improved sensitivity of the MR signal for iron that will enable applications of much lower doses and produce far greater detection.

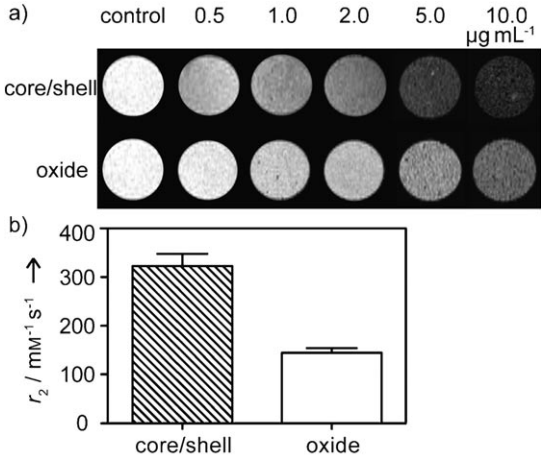

Figure 2. a) T_2-weighted MR images at 9.4 T comparing the T_2 contrast (darkening effect) from the iron/iron oxide core/shell nanoparticles and iron oxide nanoparticles in agar with Fe concentration of 0 (control), 0.5, 1.0, 2.0, 5.0, and 10.0 μg(Fe) mL^{-1}. b) Relaxivity (r_2) of the core/shell and oxide nanoparticles determined from the same samples.

To assess the clinical applicability of the NPs in vivo, the iron/iron oxide core/shell and iron oxide NPs were administered to mice and MRI experiments were performed at 1.5 T. Contrast effects of the NPs were examined at the liver, spleen, and lymph nodes. Tissues in these organs are rich in phagocytic cells and have a strong tendency to uptake circulating iron and iron oxide NPs.[19]

As shown in Figure 3 a–c, the core/shell NPs produced noticeably darker contrast than the oxide NPs for all three organs (regions indicated by arrows). The contrast effects were statistically analyzed by comparing the % reduction in the T_2 signal produced by the NPs relative to that observed for the control mice (Figure 3 d). When the core/shell NPs were used as the contrast agents, typically twice the contrast improvement was observed over the use of oxide NPs. With core/shell NPs, 45, 58 and 29 % reduction in the T_2-weighted signal were seen in the liver, spleen and lymph nodes, respectively. The corresponding signal reduction with the use of oxide NPs were 21, 29 and 17 %, respectively. The fact that contrast is improved for the mouse lymph nodes that have an average size of 1.5 mm, is particularly significant and indicates that the core/shell NPs could improve the detection of small tumors.

To investigate small tumor detection in vivo, mice bearing breast cancer cells were administered with the core/shell and oxide NPs and T_2-weighted MR images were obtained. In the MR images of the mouse that received the core/shell NPs, tumor of 1–3 mm could be unambiguously detected (Figure S3). In comparison, the contrast enhancement achieved by the oxide NPs was relatively insignificant and the tumor could not be visibly distinguished. It has been shown that the sensitivity for detecting cancerous nodes in vivo decreases to below 50 % when the tumor is smaller than 5 mm.[20] The improved tumor detection demonstrated here by the core/shell NPs holds the potential to a more effective detection of early lymph node metastases, which has a large impact on the treatment of a range of cancers.

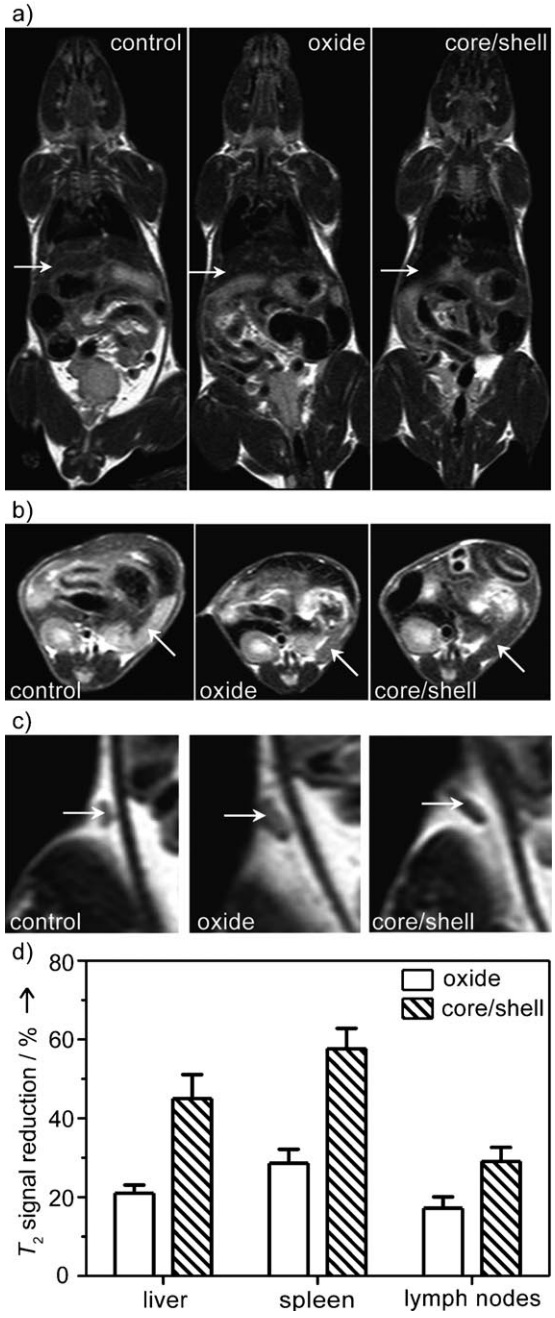

Figure 3. T_2-weighted MR images of a control mouse and mice 24 h after injection of iron oxide and iron/iron oxide core/shell nanoparticles; arrows indicate the regions of interest, where T_2 contrast was analyzed: a) coronal images with arrows indicating the liver; b) axial images at the level of spleen; c) coronal images enlarged at the left inguinal region. d) Bar graph comparing the % reduction of T_2 relative to that of control caused by the presence of oxide and core/shell nanoparticles in the liver (a), spleen (b), and lymph nodes (c).

In this study, the doses of contrast agents used are much lower than the maximum safe limit reported for mice,[21] and we found no evidence of overt toxicity or failure to thrive in any mice for up to three months after nanoparticle administration.

In summary, single-crystal iron NPs were synthesized through a straightforward solution-phase route, which involved low temperatures and without the use of highly toxic chemicals. Natural oxidation of the iron nanocrystals subsequently yielded highly crystalline iron/iron oxide core/shell NPs. These NPs are demonstrated to exhibit highly effective MR contrast enhancement in multiple organs, and to enable unambiguous detection of small tumors of 1–3 mm in vivo at 1.5 T. The improvements in MR contrast will contribute to further development and advancement of various diagnostic and therapeutic medical applications.

Experimental Section

The iron precursor $[Fe(C_5H_5)(C_6H_7)]$ was prepared according to a previously described method.[22] For the synthesis of iron nanocrystals, the iron precursor (0.4 g), OLA (2 mL, Aldrich, 98%), and mesitylene (8 mL, Aldrich, 98%) were added to a closed reaction vessel, which was then flushed three times with hydrogen gas (H_2) before being filled with 100 kPa H_2, and sealed. The bottle was placed into an oven heated at 130°C and remained for 2 days. The reaction was allowed to cool to room temperature naturally before the reaction vessel was opened to air. Ligand exchange to replace OLA with DMSA was carried out based on known methods.[23] Each synthesis typically produced 60 mg Fe, which gave approximately 50% yield.

The TEM images were taken on a JEOL 2010, operated at an acceleration voltage of 200 keV. Powder XRD measurements were conducted at the Stanford Synchrotron Radiation Lightsource at beam line 7–2, using radiation of $\lambda = 0.775$ Å. Magnetization measurements were performed on a Quantum Design SQUID magnetometer, of model MPMS-XL. MRI of NPs was performed at 9.4 T, using a Bruker Instruments AVANCE400 NMR spectrometer, equipped with a Bruker Micro 2.5 imaging module. In vivo MRI of mice was performed using a clinical 1.5-T MR scanner (Philips Medical Systems), equipped with a wrist solenoid coil.

Received: January 22, 2011
Published online: April 6, 2011

Keywords: imaging agents · iron oxide · magnetic resonance imaging · nanoparticles

[1] Q. A. Pankhurst, N. K. T. Thanh, S. K. Jones, J. Dobson, *J. Phys. D* **2009**, *42*, 224001.
[2] a) H. B. Na, I. C. Song, T. Hyeon, *Adv. Mater.* **2009**, *21*, 2133–2148; b) A. K. Gupta, M. Gupta, *Biomaterials* **2005**, *26*, 3995–4021.
[3] a) C. Corot, P. Robert, J.-M. Idee, M. Port, *Adv. Drug Delivery Rev.* **2006**, *58*, 1471–1504; b) S. Laurent, D. Forge, M. Port, A. Roch, C. Robic, L. V. Elst, R. N. Muller, *Chem. Rev.* **2008**, *108*, 2064–2110.
[4] a) Y.-w. Jun, Y.-M. Huh, J.-s. Choi, J.-H. Lee, H.-T. Song, S. Kim, S. Kim, S. Yoon, K.-S. Kim, J.-S. Shin, J.-S. Suh, J. Cheon, *J. Am. Chem. Soc.* **2005**, *127*, 5732–5733; b) J.-H. Lee, Y.-M. Huh, Y.-w. Jun, J.-w. Seo, J.-t. Jang, H.-T. Song, S. Kim, E.-J. Cho, H.-G. Yoon, J.-S. Suh, J. Cheon, *Nat. Med.* **2007**, *13*, 95–99.
[5] D. L. Huber, *Small* **2005**, *1*, 482–501.
[6] S. Peng, C. Wang, J. Xie, S. Sun, *J. Am. Chem. Soc.* **2006**, *128*, 10676.
[7] C. M. Wang, D. R. Baer, L. E. Thomas, J. E. Amonette, J. Antony, Y. Qiang, G. Duscher, *J. Appl. Phys.* **2005**, *98*, 094308.
[8] a) A. Cabot, V. F. Puntes, E. Shevchenko, Y. Yin, L. Balcells, M. A. Marcus, S. M. Hughes, A. P. Alivisatos, *J. Am. Chem. Soc.* **2007**, *129*, 10358–10360; b) H. Lee, T.-J. Yoon, R. Weissleder, *Angew. Chem.* **2009**, *121*, 5767–5770; *Angew. Chem. Int. Ed.* **2009**, *48*, 5657–5660.
[9] a) F. Dumestre, B. Chaudret, C. Amiens, P. Renaud, P. Fejes, *Science* **2004**, *303*, 821–823; b) A. Shavel, B. Rodríguez-González, M. Spasova, M. Farle, L. M. Liz-Marzán, *Adv. Funct. Mater.* **2007**, *17*, 3870–3876.
[10] D. Astruc, *Tetrahedron* **1983**, *39*, 4027–4095.
[11] a) J. Watt, N. Young, S. Haigh, A. Kirkland, R. D. Tilley, *Adv. Mater.* **2009**, *21*, 2288–2293; b) S. Cheong, J. Watt, B. Ingham, M. F. Toney, R. D. Tilley, *J. Am. Chem. Soc.* **2009**, *131*, 14590–14595.
[12] J. J. Chisolm, Jr., *Clin. Toxicol.* **2000**, *38*, 365–375.
[13] A. L. Miller, *Altern. Med. Rev.* **1998**, *3*, 199–207.
[14] M. F. Toney, A. J. Davenport, L. J. Oblonsky, M. P. Ryan, C. M. Vitus, *Phys. Rev. Lett.* **1997**, *79*, 4282–4285.
[15] H. P. Klug, L. E. Alexander, *X-ray Diffraction Procedures for Polycrystalline and Amorphous Materials*, Wiley, New York, **1974**.
[16] S. Gangopadhyay, C. G. Hadjipanayis, B. Dale, C. M. Sorensen, K. J. Klabunde, V. Papaefthymiou, A. Kostikas, *Phys. Rev. B* **1992**, *45*, 9778–9787.
[17] a) T. R. Pisanic II, J. D. Blackwell, V. I. Shubayev, R. R. Finones, S. Jin, *Biomaterials* **2007**, *28*, 2572–2581; b) H. Zhao, K. Saatchi, U. O. Hafeli, *J. Magn. Magn. Mater.* **2009**, *321*, 1356–1363.
[18] C. G. Hadjipanayis, M. J. Bonder, S. Balakrishnan, X. Wang, H. Mao, G. C. Hadjipanayis, *Small* **2008**, *4*, 1925–1929.
[19] T. K. Jain, M. K. Reddy, M. A. Morales, D. L. Leslie-Pelecky, V. Labhasetwar, *Mol. Pharm.* **2008**, *5*, 316–327.
[20] M. G. Harisinghani, J. O. Barentsz, P. F. Hahn, W. M. Deserno, S. Tabatabaei, C. H. van de Kaa, J. de La Rosette, R. Weissleder, *N. Engl. J. Med.* **2003**, *348*, 2491–2499.
[21] a) M. K. Yu, Y. Y. Jeong, J. Park, S. Park, J. W. Kim, J. J. Min, K. Kim, S. Jon, *Angew. Chem.* **2008**, *120*, 5442–5445; *Angew. Chem. Int. Ed.* **2008**, *47*, 5362–5365; b) C. Bárcena, A. K. Sra, G. S. Chaubey, C. Khemtong, J. P. Liu, J. Gao, *Chem. Commun.* **2008**, 2224–2226.
[22] M. L. H. Green, L. Pratt, G. Wilkinson, *J. Chem. Soc.* **1960**, 989–997.
[23] N. Fauconnier, J. N. Pons, J. Roger, A. Bee, *J. Colloid Interface Sci.* **1997**, *194*, 427–433.

